

HyP-NeRF: Learning Improved NeRF Priors using a HyperNetwork

Bipasha Sen*
MIT CSAIL
bise@mit.edu

Gaurav Singh*
IIIT, Hyderabad
gaurav.si@research.iiit.ac.in

Aditya Agarwal*
MIT CSAIL
adityaag@mit.edu

Rohith Agaram
IIIT, Hyderabad
rohith.agaram@research.iiit.ac.in

K Madhava Krishna
IIIT, Hyderabad
mkrishna@iiit.ac.in

Srinath Sridhar
Brown University
srinath@brown.edu

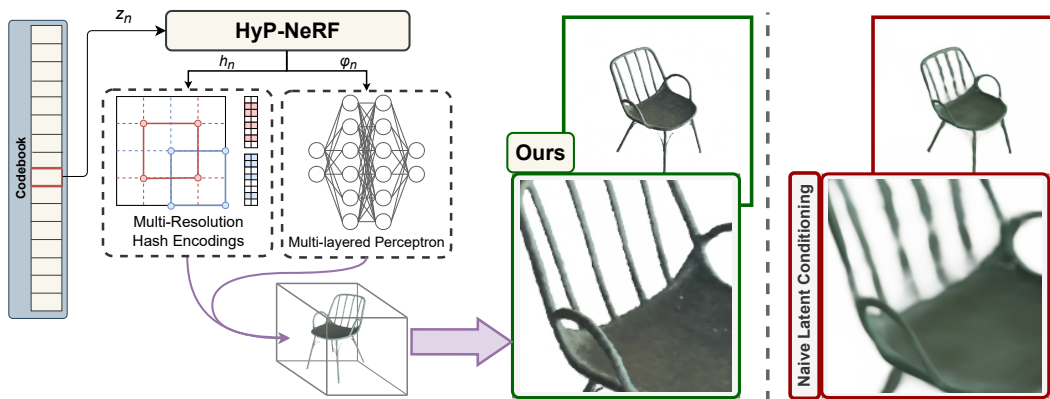


Figure 1: We propose HyP-NeRF, a latent conditioning method that learns improved quality NeRF priors using a hypernetwork to generate instance-specific multi-resolution hash encodings along with neural network weights. The figure showcases the fine details preserved in the NeRF generated by HyP-NeRF (green box) as opposed to the NeRF generated by naive conditioning (red box) in which, a hypernetwork predicts only the neural weights while relying on the standard positional encodings.

Abstract

Neural Radiance Fields (NeRF) have become an increasingly popular representation to capture high-quality appearance and shape of scenes and objects. However, learning generalizable NeRF priors over categories of scenes or objects has been challenging due to the high dimensionality of network weight space. To address the limitations of existing work on generalization, multi-view consistency and to improve quality, we propose HyP-NeRF, a latent conditioning method for learning generalizable category-level NeRF priors using hypernetworks. Rather than using hypernetworks to estimate only the weights of a NeRF, we estimate both the weights and the multi-resolution hash encodings [35] resulting in significant quality gains. To improve quality even further, we incorporate a denoise and finetune strategy that denoises images rendered from NeRFs estimated by the hypernetwork and finetunes it while retaining multiview consistency. These improvements enable us to use

*Equal authors (order decided by a coin flip)

HyP-NeRF as a generalizable prior for multiple downstream tasks including NeRF reconstruction from single-view or cluttered scenes, and text-to-NeRF. We provide qualitative comparisons and evaluate HyP-NeRF on three tasks: generalization, compression, and retrieval, demonstrating our state-of-the-art results.²

1 Introduction

Neural fields, also known as implicit neural representations (INRs), are neural networks that learn a continuous representation of physical quantities such as shape or radiance at any given space-time coordinate [70]. Recent developments in neural fields have enabled significant advances in applications such as 3D shape generation [77], novel view synthesis [32, 2], 3D reconstruction [72, 66, 38, 68], and robotics [52, 51]. In particular, we are interested in Neural Radiance Fields (NeRF) that learn the parameters of a neural network $f_\phi(\mathbf{x}, \theta) = \{\sigma, c\}$, where \mathbf{x} and θ are the location and viewing direction of a 3D point, respectively, and σ and c denote the density and color estimated by f_ϕ at that point. Once fully trained, f_ϕ can be used to render novel views of the 3D scene.

Despite their ability to model high-quality appearance, NeRFs cannot easily generalize to scenes or objects not seen during training thus limiting their broader application. Typically, achieving generalization involves learning a prior over a data source such as image, video, or point cloud distributions [21, 20, 58, 76, 29, 49], possibly belonging to a category of objects [65, 46]. However, NeRFs are continuous volumetric functions parameterized by tens of millions of parameters making it challenging to learn generalizable priors. Previous works try to address this challenge by relying on 2D image-based priors, 3D priors in voxelized space, or by using latent conditioning.

Image-based priors re-use the information learned by 2D convolutional networks [75, 34] but may lack 3D knowledge resulting in representations that are not always multiview consistent. Methods that learn 3D priors in voxelized space [33] suffer from high compute costs and inherently lower quality due to voxelization limitations. Latent conditioning methods [19, 43] learn a joint network $f(x, \theta, z)$ where z is the conditioning vector for a given object instance. These methods retain the advantages of native NeRF representations such as instance-level 3D and multiview consistency, but have limited capacity to model a diverse set of objects at high visual and geometric quality. InstantNGP [35] provides a way to improve quality and speed using *instance-specific* multi-resolution hash encodings (MRHE), however, this is limited to single instances.

We propose HyP-NeRF, a latent conditioning method for learning improved quality generalizable **category-level NeRF priors** using hypernetworks [15] (see Figure 1). We take inspiration from methods that use meta-learning to learn generalizable representations [55, 48] while retaining the quality of instance-specific methods [35]. Our hypernetwork is trained to generate the parameters—both the multi-resolution **hash encodings (MRHE) and weights**—of a NeRF model of a given category conditioned on an instance code z_n . For each instance code z_n in the learned codebook, HyP-NeRF estimates h_n denoting the instance-specific MRHE along with ϕ_n indicating the weights of an MLP. Our key insight is that estimating both the MRHEs and the weights results in a significant improvement in quality. To improve the quality even further, we denoise rendered views [42] from the estimated NeRF model, and finetune the NeRF with the denoised images to enforce multiview consistency. As shown in Figure 2 and the experiments section, this denoising and finetuning step significantly improves quality and fine details while retaining the original shape and appearance properties.

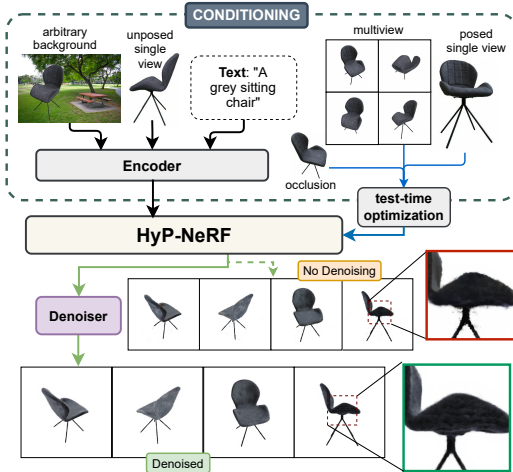


Figure 2: Once trained, HyP-NeRF acts as a prior to support multiple downstream applications, including NeRF reconstruction from single or multi-view images and cluttered scene images, and text-to-NeRF. We further improve quality using our denoising network.

²Project page: [hyp-nerf.github.io](https://github.com/hyp-nerf)

Once HyP-NeRF is trained, it can be used as a NeRF prior in a variety of different applications such as NeRF reconstruction from a single view posed or unposed images, single pass text-to-NeRF, or even the ability to reconstruct real-world objects in cluttered scene images (see Figure 2). We show qualitative results on applications and quantitatively evaluate HyP-NeRF’s performance and suitability as a NeRF prior on the ABO dataset [11] across three tasks: generalization, compression, and retrieval. To sum up our contributions:

1. We introduce HyP-NeRF, a method for learning improved quality NeRF priors using a hypernetwork that estimates *instance-specific* hash encodings and MLP weights of a NeRF.
2. We propose a denoise and finetune strategy to further improve the quality while preserving the multiview consistency of the generated NeRF.
3. We demonstrate how our NeRF priors can be used in multiple downstream tasks including single-view NeRF reconstruction, text-to-NeRF, and reconstruction from cluttered scenes.

2 Related Work

Neural Radiance Fields [32] (NeRFs) are neural networks that capture a specific 3D scene or object given sufficient views from known poses. Numerous follow-up work (see [62, 70] for a more comprehensive review) has investigated improving quality and speed, relaxing assumptions, and building generalizable priors. Strategies for improving quality or speed include better sampling [2], supporting unbounded scenes [3], extensions to larger scenes [69, 60], using hybrid representations [35, 74], using learned initializations [61, 5, 45], or discarding neural networks completely [73, 59]. Other work relaxes assumption of known poses [67, 31, 27, 25, 9, 53], or reduce the number of views [75, 43, 4, 14, 34, 44, 71, 28, 37]. Specifically, PixelNeRF [75] uses convolution-based image features to learn priors enabling NeRF reconstruction from as few as a single image. VisionNeRF [28] extends PixelNeRF by augmenting the 2D priors with 3D representations learned using a transformer. Unlike these methods, we depend purely on priors learned by meta-learning, specifically by hypernetworks [15]. AutoRF [34] and LolNeRF [43] are related works that assume only a single view for each instance at the training time. FWD [5] optimizes NeRFs from sparse views in real-time and SRT [45] aims to generate NeRFs in a single forward pass. These methods produce NeRFs of lower quality and are not designed to be used as priors for various downstream tasks. In contrast, our focus is to generate high-quality multiview consistent NeRFs that capture fine shapes and textures details. HyP-NeRF can be used as a category-level prior for multiple downstream tasks including NeRF reconstruction from one or more posed or unposed images, text-to-NeRF (similar to [40, 18]), or reconstruction from cluttered scene images. Additionally, HyP-NeRF can estimate the NeRFs in a single forward pass with only a few iterations needed to improve the quality. Concurrent to our work, NerfDiff [13] and SSDNeRF [8] achieve high quality novel view synthesis by using diffusion models.

Learning 3D Priors. To learn category-level priors, methods like CodeNeRF [19] and LolNeRF [43] use a conditional NeRF on instance vectors z given as $f(x, \theta, z)$, where different z s result in different NeRFs. PixelNeRF [75] depends on 2D priors learned by 2D convolutional networks which could result in multi-view inconsistency. DiffRF [33] uses diffusion to learn a prior over voxelized radiance field. Like us, DiffRF can generate radiance fields from queries like text or images. However, it cannot be directly used for downstream tasks easily.

Our approach closely follows the line of work that aims to learn a prior over a 3D data distribution like signed distance fields [39], light field [55], and videos [48]. We use meta-learning, specifically hypernetworks [15], to learn a prior over the MRHEs and MLP weights of a fixed NeRF architecture. LearnedInit [61], also employs standard meta-learning algorithms for getting a good initialization of the NeRF parameters. However, unlike us, they do not use a hypernetwork, and use the meta-learning algorithms only for initializing a NeRF, which is further finetuned on the multiview images. Methods like GRAF [47], π -GAN [6], CIPS-3D [79], EG3D [7], and Pix2NeRF [4] use adversarial training setups with 2D discriminators resulting in 3D and multiview inconsistency. [40, 64, 16] tightly couple text and NeRF priors to generate and edit NeRFs based on text inputs. We, on the other hand, train a 3D prior on NeRFs and separately train a mapping network that maps text to HyP-NeRF’s prior, decoupling the two.

3 HyP-NeRF: Learning Improved NeRF prior using a Hypernetwork

Our goal is to learn a generalizable NeRF prior for a category of objects while maintaining visual and geometric quality, and multiview consistency. We also want to demonstrate how this prior can be used to enable downstream applications in single/few-image NeRF generation, text-to-NeRF, and reconstruction of real-world objects in cluttered scenes.

Background. We first provide a brief summary of hypernetworks and multi-resolution hash encodings that form the basis of HyP-NeRF. Hypernetworks are neural networks that were introduced as a meta-network to predict the weights for a second neural network. They have been widely used for diverse tasks, starting from representation learning for continuous signals [55, 54, 57, 48], compression [36, 12], few-shot learning [50, 23], continual learning [63]. Our key insight is to use hypernetworks to generate both the network weights and instance-specific MRHEs.

Neural Radiance Fields (NeRF) [32, 2] learn the parameters of a neural network $f_\phi(\mathbf{x}, \theta) = \{\sigma, c\}$, where \mathbf{x} and θ are the location and viewing direction of a 3D point, respectively, and σ and c denote the density and color predicted by f_ϕ at that point. Once fully trained, f_ϕ can be used to render novel views of the 3D scene. NeRF introduced *positional encodings* of the input 3D coordinates, \mathbf{x} , to a higher dimensional space to capture high-frequency variations in color and geometry. InstantNGP [35] further extended this idea to *instance-specific* multi-resolution hash encodings (MRHE) to encode \mathbf{x} dynamically based on scene properties. These MRHEs, h , are learned along with the MLP parameters, ϕ for a given NeRF function, f and show improved quality and reduced training/inference time.

Image Denoising is the process of reducing the noise and improving the perceptual quality of images while preserving important structural details. Recent advancements in deep learning-based image restoration and denoising techniques [26, 24, 10] have demonstrated remarkable success in removing noise and enhancing the perceptual quality of noisy images that may have suffered degradation. Such networks are trained on large datasets of paired noisy and clean images to learn a mapping between the degraded input and the corresponding high-quality output by minimizing the difference between the restored and the ground truth clean image. In our case, we use denoising to improve the quality of our NeRF renderings by reducing artifacts and improving the texture and structure at the image level.

3.1 Method

Given a set of NeRFs denoted by $\{f_{(\phi_n, h_n)}\}_{n=1}^N$, where N denotes the number of object instances in a given object category, we want to learn a prior $\Phi = \{\Phi_S, \Phi_C\}$, where Φ_S and Φ_C are the shape and color priors, respectively. Each NeRF, $f_{(\cdot)_n}$, is parameterized by the neural network weights, ϕ_n , and learnable MRHEs, h_n as proposed in [35]. $f_{(\cdot)_n}$ takes a 3D position, \mathbf{x} , and viewing direction, θ , as input and predicts the density conditioned on \mathbf{x} denoted by $\sigma_n^{\{\mathbf{x}\}}$, and color conditioned on \mathbf{x} and θ denoted by $c_n^{\{\mathbf{x}, \theta\}}$. This is given as,

$$f_{(\phi_n, h_n)}(\mathbf{x}, \theta) = \{\sigma_n^{\{\mathbf{x}\}}, c_n^{\{\mathbf{x}, \theta\}}\}. \tag{1}$$

Our proposed method for learning NeRF priors involves two steps. First, we train a hypernetwork, M , to learn a prior over a set of multiview consistent NeRFs of high-quality shape and texture. Second, we employ an image-based denoising network that takes as input an already multiview consistent set of images, rendered from the predicted NeRF, and improves the shape and texture of NeRF to higher quality by finetuning on a set of denoised images. Our architecture is outlined in Figure 3 and we explain each step in detail below.

Step 1: Hypernetwork for Learning NeRF Prior. We want to design our hypernetwork, M , with trainable parameters, Ω that can predict NeRF parameters $\{\phi_n, h_n\}$ given a conditioning code $z_n = \{S_n, C_n\}$, where S_n and C_n are the shape and color codes, respectively, for an object instance n belonging to a specific category. Here, S_n and C_n belong to codebooks, S and C that are trained along with Ω in an auto-decoding fashion.

As shown in Figure 3 (top), ideally we want M to learn a prior $\{\Phi_C, \Phi_S\}$ over S and C such that given a random set of codes, $\{\mathcal{Y}_S \sim \Phi_S, \mathcal{Y}_C \sim \Phi_C\}$, M should be able to generate a valid NeRF with consistent shape and texture for the given category of objects. To achieve this, we train M by assuming the same constraints as are needed to train a NeRF - a set of multiview consistent images $\mathbf{I} = \{\{I_{\theta \in \Theta}\}_n\}_{n=1}^N$ for a set of poses, Θ . In each training step, we start with a random object instance, n , and use the corresponding codes S_n and C_n from the codebooks as an input for M . Our

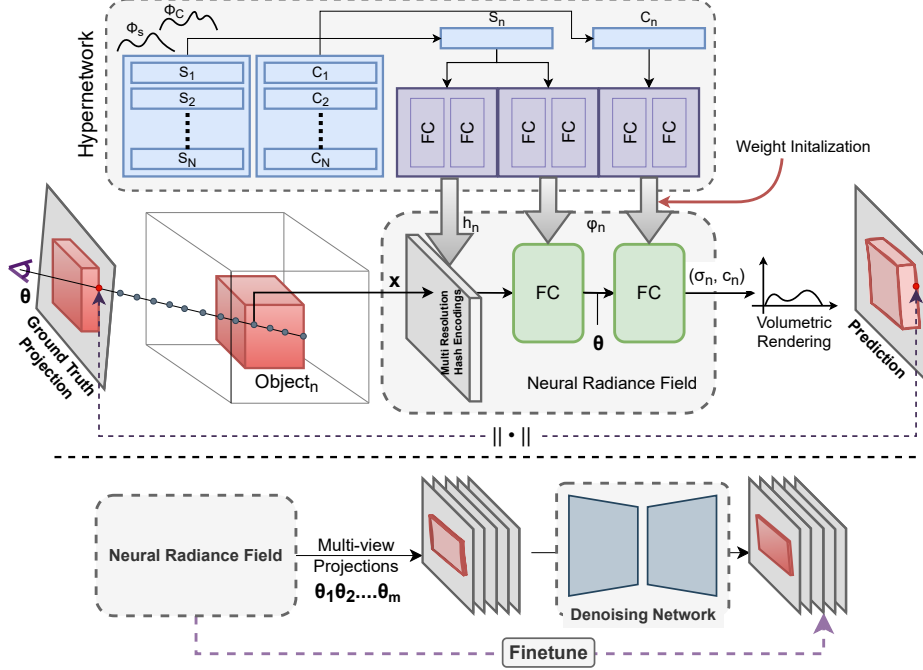


Figure 3: **Architecture Diagram:** HyP-NeRF is trained and inferred in two steps. In the first step (**top**), our hypernetwork, M , is trained to predict the parameters of a NeRF model, f_n corresponding to object instance n . At this stage, the NeRF model acts as a set of differentiable layers to compute the volumetric rendering loss, using which M is trained on a set of N objects, thereby learning a prior $\Phi = \{\Phi_S, \Phi_C\}$ over the shape and color codes given by S and C , respectively. In the second step (**bottom**), the quality of the predicted multiview consistent NeRF, f_n , is improved using a denoising network trained directly in the image space. To do this, f_n is rendered from multiple known poses to a set of images that are improved to photorealistic quality. f_n is then finetuned on these improved images. Importantly, since f_n is only finetuned and not optimized from scratch, and thus f_n retains the multiview consistency whilst improving in terms of texture and shape quality.

key insight is that estimating **both** the MRHEs and MLP weights results in a higher quality than other alternatives. M then predicts the NeRF parameters $\{\phi_n, h_n\}$, which is then used to minimize the following objective:

$$\mathcal{L}(\Omega, S_n, C_n) = \sum_{\mathbf{r} \in R} \|\mathbf{V}'(\mathbf{r}, \{\sigma_n^{x_i^r}, c_n^{x_i^r, \theta}\}_{i=1}^L) - \mathbf{V}_n(\mathbf{r})\| \quad (2)$$

$$\{\sigma_n^{x_i^r}, c_n^{x_i^r, \theta}\} = f_{(\phi_n, h_n)}(x_i^r, \theta) \quad \text{and} \quad \{\phi_n, h_n\} = M_\Omega(S_n, C_n) \quad (3)$$

where \mathbf{V}' denotes the volumetric rendering function as given in [32] eqn. 3 and 5, \mathbf{r} is a ray projected along the camera pose θ , $x_i^r \in \mathbf{x}$ and L denote the number of points sampled along \mathbf{r} , and \mathbf{V}_n denote the ground truth value for projection of the n^{th} object along \mathbf{r} .

Note that, in this step, the only trainable parameters are the meta-network weights, Ω , and the codebooks S and C . In this setting, the NeRF functions $f_{(\cdot)_n}$ only act as differentiable layers that allow backpropagation through to M enabling it to train with multiview consistency loss attained by the volumetric rendering loss as described in [32]. We use an instantiation of InstantNGP [35] as our function $f_{(\cdot)_n}$ consisting of MRHE and a small MLP.

A general limitation of hypernetworks arises from the fact that the intended output space (i.e. the space of valid MLP weight matrices) is a subset of the actual output space, which is unrestricted and can be any 2D matrix. Thus, a hypernetwork trained on loss functions in the weight space can result in unstable training, and might require a lot of training examples to converge. To overcome this issue, we train our hypernetwork end-to-end directly on images, so that it learns the implicit NeRF space along with the category specific prior on it, which simplifies the setting for the hypernetwork and

allows for more stable training. As a causal effect of this, HyP-NeRF, when trained on less number of examples, essentially acts as a compressing model.

Step 2: Denoise and Finetune. In the first step, M is trained to produce a consistent NeRF with high-fidelity texture and shape. However, we observed that there is room to improve the generated NeRFs to better capture fine details like uneven textures and edge definition. To tackle this challenge, we augment M using a denoising process that takes $f_{(\cdot)_n}$ and further finetunes it to achieve $f_{(\cdot)_n}^H$.

As shown in Figure 3 (bottom), we render novel views from the multiview consistent NeRF into m different predefined poses given by $\{\theta_1, \theta_2 \dots \theta_m\}$ to produce a set of multiview consistent images $\{\hat{I}_i\}_{i=1}^m$. We then use a pre-trained image-level denoising autoencoder that takes $\{\hat{I}_i\}_{i=1}^m$ as input and produces images of improved quality given as $\{\hat{I}_i^H\}_{i=1}^m$. These improved images are then used to finetune $f_{(\cdot)_n}$ to achieve $f_{(\cdot)_n}^H$. Note that, we do not train the NeRFs from scratch on $\{\hat{I}^H\}$ and only finetune the NeRFs, which ensures fast optimization and simplifies the task of the denoising module that only needs to improve the quality and does not necessarily need to maintain the multiview consistency. While our denoising is image-level, we still obtain multiview consistent NeRFs since we finetune on the NeRF itself (as we also demonstrate through experiments in the Appendix).

For our denoising autoencoder, we use VQVAE2 [42] as the backbone. To train this network, we simply use images projected from the NeRF, predicted by the hypernetwork (lower quality relative to the ground truth) as the input to the VQVAE2 model. We then train VQVAE2 to decode the ground truth by minimizing the L2 loss objective between VQVAE2’s output and the ground truth.

3.2 HyP-NeRF Inference and Applications

Training over many NeRF instances, M learns a prior Φ that can be used to generate novel consistent NeRFs. However, Φ is not a known distribution like Gaussian distributions that can be naively queried by sampling a random point from the underlying distribution. We tackle this in two ways:

Test Time Optimization. In this method, given a single-view or multi-view posed image(s), we aim to estimate shape and color codes $\{S_o, C_o\}$ of the NeRF that renders the view(s). To achieve this, we freeze M ’s parameters and optimize the $\{S_o, C_o\}$ using the objective given in Equation (2).

Query Network. We create a query network, Δ , that maps a point from a known distribution to Φ . As CLIP’s [41] pretrained semantic space, say \mathbf{C} , is both text and image aware, we chose \mathbf{C} , as our known distribution and learn a mapping function $\Delta(z \sim \mathbf{C}) \rightarrow \Phi$. Here, Δ is an MLP that takes z as input and produces $\mathcal{Y}_z \in \Phi$ as output. To train Δ , we randomly sample one pose from the ground truth multiview images $I_\theta^n \in \{I_{\theta \in \Theta}\}_n$ and compute the semantic embedding $z_\theta^n = \text{CLIP}(I_\theta^n)$ and map it to $\{S_n, C_n\} \in \Phi$ given as $\{S_n, C_n\} = \Delta(z_\theta^n)$. We then train our query network by minimizing the following objective:

$$\mathcal{L}_\Delta = \sum_{\theta} \|\{S_n, C_n\} - \Delta(z_\theta^n)\|. \quad (4)$$

At the time of inference, given a text or image modality such as a text prompt, single-view unposed (in-the-wild) image, or segmented image, we compute the semantic embedding using CLIP encoder and map it to Φ using Δ , from which we obtain the shape and color codes as input for the HyP-NeRF.

Note that for N query points in a scene, the forward pass through the hypernetwork (computationally expensive) happens only once per scene. Only the NeRF predicted by the hypernetwork (computationally less expensive) is run for each query point.

4 Experiments

We provide evaluations of the prior learned by HyP-NeRF specifically focusing on the quality of the generated NeRFs. We consider three dimensions: (1) **Generalization** (Section 4.1): we validate whether HyP-NeRF can generate novel NeRFs not seen during training by conditioning on only a single-posed-view of novel NeRF instances. (2) **Compression** (Section 4.2): since HyP-NeRF is trained in an auto-decoding fashion on specific NeRF instances (see Equation (2)), we can evaluate the quality of the NeRFs compressed in this process. (3) **Retrieval** (Section 4.3): as shown in Figure 2, HyP-NeRF’s prior enables various downstream applications. We show how to combine our prior with CLIP [41] to retrieve novel NeRFs.

		Chairs				Sofa			
		PSNR↑	SSIM↑	LPIPS↓	FID↓	PSNR↑	SSIM↑	LPIPS↓	FID↓
ABO-512	PixelNeRF [75]	18.30	0.83	0.31	292.32	17.51	0.84	0.28	323.89
	CodeNeRF [19]	19.86	0.87	0.298	-	19.56	0.87	0.290	-
	HyP-NeRF (Ours)	24.23	0.91	0.16	68.11	23.96	0.90	0.18	120.80
	w/o Denoise	23.05	0.90	0.16	102.45	23.54	0.90	0.174	121.69

Table 1: **Generalization.** Comparison of single-posed-view NeRF generation. Metrics are computed on renderings of resolution 512×512 . HyP-NeRF significantly outperforms PixelNeRF and CodeNeRF on all the metrics in both the datasets.

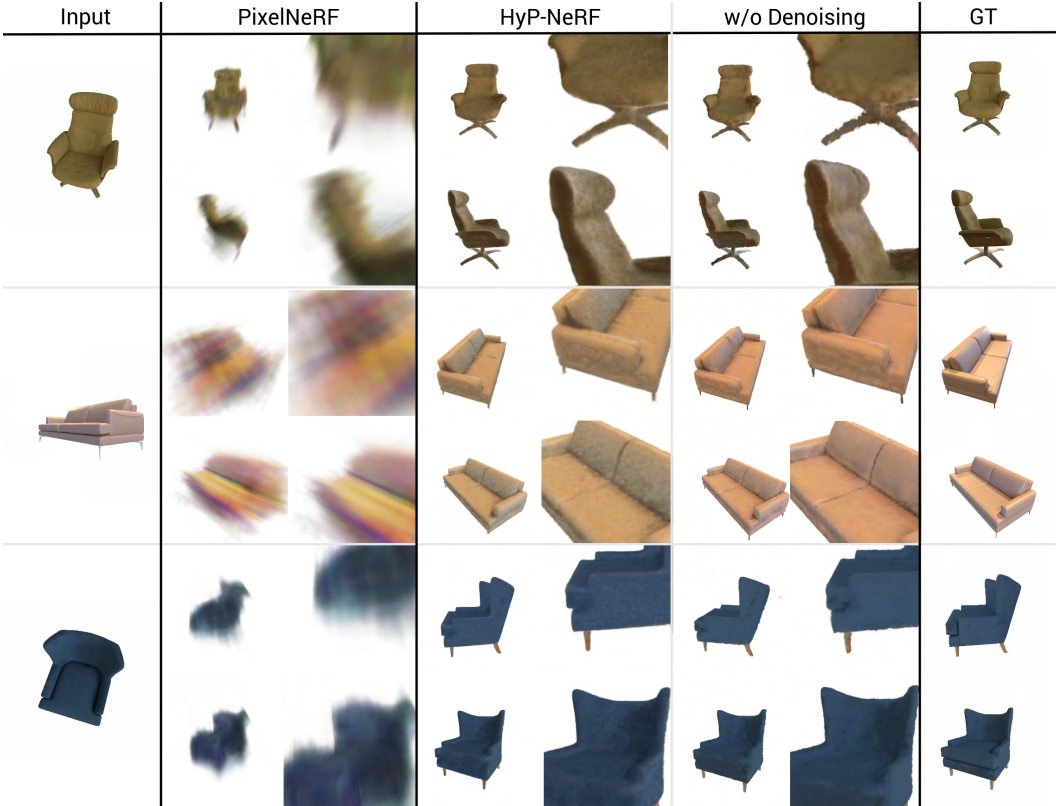


Figure 4: **Qualitative Comparison of Generalization on ABO.** The NeRFs are rendered at a resolution of 512×512 . HyP-NeRF is able to preserve fine details such as the legs, creases, and texture even for novel instances. PixelNeRF fails to preserve details and to model the structure.

Datasets and Comparisons. We primarily compare against two baselines, PixelNeRF [75] and InstantNGP [35] on the Amazon-Berkeley Objects (ABO) [11] dataset. ABO contains diverse and detailed objects rendered at a resolution of 512×512 which is perfect to showcase the quality of the NeRF generated by HyP-NeRF. Rather than use a computationally expensive model like VisionNeRF (on the SRN [56] dataset) on a resolution of 128×128 , we show our results on 512×512 and compare with PixelNeRF. Additionally, we compare with the other baselines on SRN at 128×128 resolution qualitatively in the main paper (Figure 5) and quantitatively in the Appendix. For compression, we directly compare with InstantNGP [35], that proposed MRHE, trained to fit on individual objects instance-by-instance.

Architectural Details. We use InstantNGP as $f_{(\cdot)_n}$, with 16 levels, hashtable size of 2^{11} , feature dimension of 2, and linear interpolation for computing the MRHE; the MLP has a total of 5, 64-dimensional, layers. We observed that a hashtable size 2^{11} produces NeRF of high-quality at par with the a size of 2^{14} . Hence, we use 2^{11} to speed up our training. Our hypernetwork, M , consists of 6 MLPs, 1 for predicting the MRHE, and the rest predicts the parameters ϕ for each of the MLP layers of f . Each of the MLPs are made of 3, 512-dimensional, layers. We perform all of our experiments on NVIDIA RTX 2080Tis.

	ABO Chairs				ABO Table				ABO Sofas			
	PSNR \uparrow	SSIM \uparrow	LPIPS \downarrow	CD \downarrow	PSNR \uparrow	SSIM \uparrow	LPIPS \downarrow	CD \downarrow	PSNR \uparrow	SSIM \uparrow	LPIPS \downarrow	CD \downarrow
[35]	35.43	0.96	0.07	—	34.07	0.95	0.07	—	33.87	0.95	0.08	—
Ours	31.37	0.94	0.1	0.0082	29.52	0.93	0.11	0.0033	30.32	0.94	0.11	0.0118

Table 2: **Compression.** We randomly sample 250 datapoints from our training dataset and compare the NeRFs learned using InstantNGP [35] on the individual instances against HyP-NeRF that learns the entire dataset. Note, we do not employ the denoising module (see Section 3.1) for this evaluation.

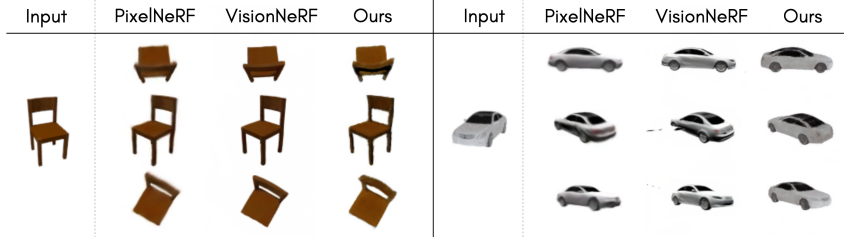


Figure 5: **Qualitative Comparison of Generalization on SRN** on the task of single-view inversion (posed in our case) and compare the quality of the views rendered at 128×128 . HyP-NeRF renders NeRFs of similar quality to the PixelNeRF and VisionNeRF baselines.

Metrics. To evaluate NeRF quality, we render them at 91 distinct views and compute metrics on the rendered images. Following PixelNeRF, we use PSNR(\uparrow), SSIM(\uparrow), and LPIPS(\downarrow) [78]. Additionally, we compute Fréchet Inception Distance (FID)(\downarrow) [17] to further test the visual quality. Although these metrics measure the quality of novel-view synthesis, they do not necessarily evaluate the geometry captured by the NeRFs. Therefore, we compute Chamfer’s Distance (CD) whenever necessary by extracting a mesh from NeRF densities [30]. Please see the Appendix for additional details.

ABO Chairs		ABO Sofa	
Top 1	Top 3	Top 1	Top 3
98.72%	99.81%	91.6%	95.27%

Table 3: **Retrieval.** We design a simple query network (see Section 3.2) to retrieve NeRF instances from HyP-NeRF’s prior seen at the time of training and achieve almost 100% accuracy.

4.1 Generalization

One way to evaluate if HyP-NeRF can render novel NeRF instances of high quality is through unconditional sampling. However, our learned prior Φ is a non-standard prior (like a Gaussian distribution) and thus random sampling needs carefully designed mapping between such a known prior and Φ . Therefore, we instead rely on a conditional task of single-view novel NeRF generation: given a single arbitrarily-chosen view of a novel object, we generate the corresponding NeRF, $f_{(\cdot)}_{\circ}$ through test-time optimization (see Section 3.2). We compare quantitatively with PixelNeRF on ABO at a high resolution of 512×512 and qualitatively with the rest of the baselines on SRN at 128×128 .

As shown in Table 1, we significantly outperform PixelNeRF on all of the metrics. Further, the qualitative results in Figure 4 clearly shows the difference between the rendering quality of HyP-NeRF against PixelNeRF. Specifically, PixelNeRF fails to learn details, especially for the Sofa category. On the other hand, HyP-NeRF preserves intricate details like the texture, legs, and folds in the objects even at a high resolution. Further, we show our results on the widely used SRN dataset at the resolution of 128×128 in Figure 5. Here, our quality is comparable with the baselines.

4.2 Compression

Unlike InstantNGP, which is trained on a single 3D instance, HyP-NeRF is trained on many NeRF instances which effectively results in the compression of these NeRFs into the latent space (or the codebook). We evaluate this compression capability by computing NeRF quality degradation compared to single-instance-only method, InstantNGP.

We randomly sample 250 instances from the training set and train InstantNGP separately on each of them. These samples are a subset of the training data used in HyP-NeRF’s codebook. We show degradation metrics in Table 2. Note that we **do not perform denoising** on the generated NeRFs as we want to only evaluate the compression component of HyP-NeRF in this section. As can be seen in Table 2, there is a significant degradation in terms of PSNR (an average of 11%), but the overall geometry is preserved almost as well as InstantNGP. However, InstantNGP is trained on a

single instance, whereas we train on 1000s of NeRF instances (1038, 783, and 517 instances for ABO Chairs, Sofa, and Tables, respectively). This results in a $60\times$ compression gain: for ABO Chairs, with 1038 training instances, HyP-NeRF needs 163MB to store the model, whereas a single instance of InstantNGP needs on average 8.9MB. Note that we use the same network architecture [1] for HyP-NeRF and InstantNGP making this a fair comparison. Moreover, the storage complexity for InstantNGP-based NeRFs is linear with respect to the number of instances, whereas our degradation in visual quality is sublinear.

4.3 Retrieval

A generalizable learned prior has the ability to generate NeRFs based on different input modalities like text, images, segmented and occluded images, random noise, and multi-view images. We now demonstrate additional querying and retrieval capabilities as described in Section 3.2.

This experiment’s goal is to retrieve specific NeRF instances that HyP-NeRF has encountered during training from a single-view unposed image of that instance. Section 4.3 presents the number of times we could correctly retrieve from an arbitrary view of seen NeRF instances. We achieve almost 100% accuracy for Chair and Sofa datasets. However, we take this a step further and try to retrieve the closest training instance code corresponding to **unseen views** of seen instances taken from in-the-wild internet images. Figure 6 (top) shows examples from this experiment in which we are able to retrieve a NeRF closely matching the input query. This demonstrates the ease of designing a simple mapping network that can effectively interact with HyP-NeRF’s prior.

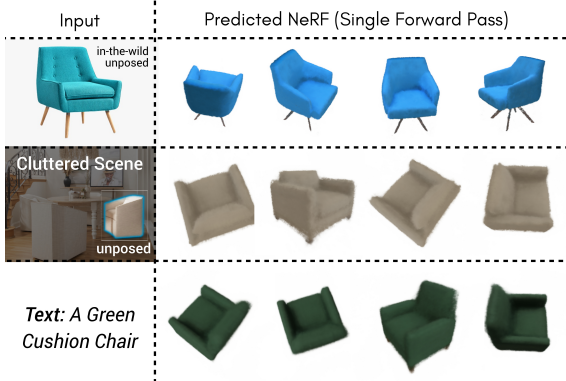


Figure 6: **Qualitative Comparison of Querying (Section 3.2) on HyP-NeRF’s prior.** In the top, we use an in-the-wild single-view unposed image to retrieve the closest NeRF HyP-NeRF has seen during training. In middle, we take a cluttered scene, and mask out the object of interest using Segment Anything [22] and in the bottom we use a text prompt as an input to our query network, Δ . We then obtain the latent codes $\{S, C\}$ from Δ , which are used as an input for HyP-NeRF.

Along with retrieving a seen instance, we use the query network to generate novel NeRFs of **unseen instances** as shown in Figure 6 (middle and bottom). In the middle row, we take an image of a cluttered scene, segment it with SAM [22], and pass this as input to the query network, from which we obtain a set of latent codes given as input to HyP-NeRF (see Figure 2). Finally, in the bottom row, we show text-to-NeRF capabilities enabled by HyP-NeRF.

4.4 Ablation

Two key designs of HyP-NeRF include incorporating the MRHE and the denoising network. We present the affect of removing these two components in Table 4 and Figure 1 for MRHE and Table 1, Figure 2, and Figure 4 for denoising. In the first ablation, we change the design of our neural network by using a hypernetwork to predict the parameters of a standard nerf with positional encodings [32]. Since we remove the MRHE, we also increase the number of layers in the MLP to match the layers mentioned in [32]. Since there is a significant increase in the view rendering time, we randomly sample 70 training examples for evaluation. As seen in Table 4, the quality of the rendered views lags significantly in all the metrics including the CD (measured against NeRFs rendered on InstantNGP individually). This is showcased visually in Figure 1 and the Appendix. Similarly, we find significant differences between the quality of the NeRFs before and after denoising (Table 1, Figure 2, and Figure 4), particularly in the Chair category with more diverse shapes.

	Chairs			
	PSNR \uparrow	SSIM \uparrow	LPIPS \downarrow	CD \downarrow
HyP-NeRF	29.23	0.94	0.10	0.0075
w/o MRHE	26.42	0.92	0.16	0.0100

Table 4: **Ablation of removing MRHE** on ABO dataset. Due to the significant rendering time of HyP-NeRF w/o MRHE, we sample 70 object instances from the training dataset to compute the metrics at 512×512 resolution.



Figure 7: Qualitative results on color and geometry disentanglement: We take two instances from the training set and switch the geometry and color codes to generate novel instances. As can be seen, the geometry and the color are transferred while preserving fine shape details. Even the fine details, like stripes and color-contrast between the chair seats and edges from Chair-2, are accurately transferred to Chair-1 (Chair-2-Geometry + Chair-1-Color). **Zoom in for an improved experience.**

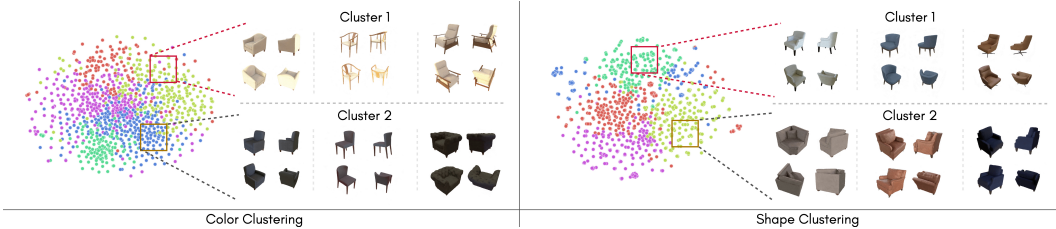


Figure 8: Latent visualization through TSNE plots on shape and color codes (from the codebooks S and C). As can be seen, the underlying space forms meaningful clusters as shown through examples randomly sampled from two different clusters.

4.5 Color and Shape Disentanglement

We start with two object instances from the train set - A and B and denote their corresponding shape and color codes as A_s, B_s and A_c, B_c . We switch the color and shape code and generate two novel NeRFs given by A_s, B_c and B_s, A_c . In Figure 7, we can clearly see the disentanglement: geometry is perfectly preserved, and the color is transferred faithfully across the NeRFs. In Figure 8, we show clusters of color and shape codes using TSNE plots and visualize instances from the clusters.

5 Conclusion, Limitation, and Future Work

We propose HyP-NeRF, a learned prior for Neural Radiance Fields (NeRFs). HyP-NeRF uses a hypernetwork to predict instance-specific multi-resolution hash encodings (MRHEs) that significantly improve the visual quality of the predicted NeRFs. To further improve the visual quality, we propose a denoising and finetuning technique that result in an improved NeRF that preserves its original multiview and geometric consistency. Experimental results demonstrate HyP-NeRF’s capability to generalize to unseen samples and its effectiveness in compression. With its ability to overcome limitations of existing approaches, such as rendering at high resolution and multiview consistency, HyP-NeRF holds promise for various applications as we demonstrate for single- and multi-view NeRF reconstruction and text-to-NeRF.

Limitation and Future Work. One limitation of our work is the need for the pose to be known during test-time optimization (Section 3.2). Although we propose the query network to predict novel NeRFs conditioned on an unposed single view, the result may not exactly match the given view because of the loss of detail in the CLIP embedding. Future work should design a mapping network that can preserve fine details. An iterative pose refinement approach that predicts the pose along with the shape and color codes could also be adopted. A second limitation of our work is the non-standard prior Φ that was learned by HyP-NeRF which makes unconditional generation challenging. GAN-based generative approaches solve this problem by randomly sampling from a standard distribution (like Gaussian distribution) and adversarially training the network. However, those methods often focus more on image quality than 3D structure. Future work could address this by incorporating latent diffusion models that can map a standard prior to HyP-NeRF’s prior.

References

- [1] GitHub - ashawkey/torch-ngp: A pytorch CUDA extension implementation of instant-ngp (sdf and nerf), with a GUI. — github.com. <https://github.com/ashawkey/torch-ngp>. [Accessed 17-May-2023].
- [2] Jonathan T. Barron, Ben Mildenhall, Matthew Tancik, Peter Hedman, Ricardo Martin-Brualla, and Pratul P. Srinivasan. Mip-nerf: A multiscale representation for anti-aliasing neural radiance fields. *ICCV*, 2021.
- [3] Jonathan T. Barron, Ben Mildenhall, Dor Verbin, Pratul P. Srinivasan, and Peter Hedman. Mip-nerf 360: Unbounded anti-aliased neural radiance fields. *CVPR*, 2022.
- [4] Shengqu Cai, Anton Obukhov, Dengxin Dai, and Luc Van Gool. Pix2nerf: Unsupervised conditional p-gan for single image to neural radiance fields translation. In *Proceedings of the IEEE/CVF Conference on Computer Vision and Pattern Recognition (CVPR)*, pages 3981–3990, June 2022.
- [5] Ang Cao, Chris Rockwell, and Justin Johnson. Fwd: Real-time novel view synthesis with forward warping and depth. *CVPR*, 2022.
- [6] Eric Chan, Marco Monteiro, Petr Kellnhofer, Jiajun Wu, and Gordon Wetzstein. pi-gan: Periodic implicit generative adversarial networks for 3d-aware image synthesis. In *Proc. CVPR*, 2021.
- [7] Eric R. Chan, Connor Z. Lin, Matthew A. Chan, Koki Nagano, Boxiao Pan, Shalini De Mello, Orazio Gallo, Leonidas Guibas, Jonathan Tremblay, Sameh Khamis, Tero Karras, and Gordon Wetzstein. Efficient geometry-aware 3D generative adversarial networks. In *arXiv*, 2021.
- [8] Hansheng Chen, Jiatao Gu, Anpei Chen, Wei Tian, Zhuowen Tu, Lingjie Liu, and Hao Su. Single-stage diffusion nerf: A unified approach to 3d generation and reconstruction. In *ICCV*, 2023.
- [9] Shin-Fang Chng, Sameera Ramasinghe, Jamie Sherrah, and Simon Lucey. Garf: gaussian activated radiance fields for high fidelity reconstruction and pose estimation. *arXiv e-prints*, pages arXiv–2204, 2022.
- [10] Jian Zhang Chong Mou, Qian Wang. Deep generalized unfolding networks for image restoration. In *IEEE Conference on Computer Vision and Pattern Recognition (CVPR)*, 2022.
- [11] Jasmine Collins, Shubham Goel, Kenan Deng, Achleshwar Luthra, Leon Xu, Erhan Gundogdu, Xi Zhang, Tomas F Yago Vicente, Thomas Dideriksen, Himanshu Arora, Matthieu Guillaumin, and Jitendra Malik. Abo: Dataset and benchmarks for real-world 3d object understanding. *CVPR*, 2022.
- [12] Shangqian Gao, Feihu Huang, and Heng Huang. Model compression via hyper-structure network, 2021.
- [13] Jiatao Gu, Alex Trevithick, Kai-En Lin, Josh Susskind, Christian Theobalt, Lingjie Liu, and Ravi Ramamoorthi. Nerfdiff: Single-image view synthesis with nerf-guided distillation from 3d-aware diffusion. In *International Conference on Machine Learning*, 2023.
- [14] Pengsheng Guo, Miguel Angel Bautista, Alex Colburn, Liang Yang, Daniel Ulbricht, Joshua M Susskind, and Qi Shan. Fast and explicit neural view synthesis. In *Proceedings of the IEEE/CVF Winter Conference on Applications of Computer Vision*, pages 3791–3800, 2022.
- [15] David Ha, Andrew Dai, and Quoc V Le. Hypernetworks. *arXiv preprint arXiv:1609.09106*, 2016.
- [16] Ayaan Haque, Matthew Tancik, Alexei Efros, Aleksander Holynski, and Angjoo Kanazawa. Instruct-nerf2nerf: Editing 3d scenes with instructions. 2023.
- [17] Martin Heusel, Hubert Ramsauer, Thomas Unterthiner, Bernhard Nessler, and Sepp Hochreiter. Gans trained by a two time-scale update rule converge to a local nash equilibrium. *Advances in neural information processing systems*, 30, 2017.
- [18] Ajay Jain, Ben Mildenhall, Jonathan T Barron, Pieter Abbeel, and Ben Poole. Zero-shot text-guided object generation with dream fields. In *Proceedings of the IEEE/CVF Conference on Computer Vision and Pattern Recognition*, pages 867–876, 2022.
- [19] Wonbong Jang and Lourdes Agapito. Codenerf: Disentangled neural radiance fields for object categories. In *Proceedings of the IEEE/CVF International Conference on Computer Vision*, pages 12949–12958, 2021.

- [20] Tero Karras, Miika Aittala, Janne Hellsten, Samuli Laine, Jaakko Lehtinen, and Timo Aila. Training generative adversarial networks with limited data. *ArXiv*, abs/2006.06676, 2020.
- [21] Tero Karras, Samuli Laine, and Timo Aila. A style-based generator architecture for generative adversarial networks. In *Proceedings of the IEEE/CVF conference on computer vision and pattern recognition*, pages 4401–4410, 2019.
- [22] Alexander Kirillov, Eric Mintun, Nikhila Ravi, Hanzi Mao, Chloe Rolland, Laura Gustafson, Tete Xiao, Spencer Whitehead, Alexander C. Berg, Wan-Yen Lo, Piotr Dollár, and Ross Girshick. Segment anything. *arXiv:2304.02643*, 2023.
- [23] A. Lamb, Evgeny S. Saveliev, Yingzhen Li, Sebastian Tschiatschek, Camilla Longden, Simon Woodhead, José Miguel Hernández-Lobato, Richard E. Turner, Pashmina Cameron, and Cheng Zhang. Contextual hypernetworks for novel feature adaptation. *ArXiv*, abs/2104.05860, 2021.
- [24] Fei Li, Lingfeng Shen, Yang Mi, and Zhenbo Li. Drcnet: Dynamic image restoration contrastive network. In Shai Avidan, Gabriel Brostow, Moustapha Cissé, Giovanni Maria Farinella, and Tal Hassner, editors, *Computer Vision – ECCV 2022*, pages 514–532, Cham, 2022. Springer Nature Switzerland.
- [25] Fu Li, Hao Yu, Ivan Shugurov, Benjamin Busam, Shaowu Yang, and Slobodan Ilic. Nerf-pose: A first-reconstruct-then-regress approach for weakly-supervised 6d object pose estimation. *arXiv preprint arXiv:2203.04802*, 2022.
- [26] Jingyun Liang, Jiezhong Cao, Guolei Sun, Kai Zhang, Luc Van Gool, and Radu Timofte. Swinir: Image restoration using swin transformer. *arXiv preprint arXiv:2108.10257*, 2021.
- [27] Chen-Hsuan Lin, Wei-Chiu Ma, Antonio Torralba, and Simon Lucey. Barf: Bundle-adjusting neural radiance fields. In *Proceedings of the IEEE/CVF International Conference on Computer Vision (ICCV)*, pages 5741–5751, October 2021.
- [28] Kai-En Lin, Lin Yen-Chen, Wei-Sheng Lai, Tsung-Yi Lin, Yi-Chang Shih, and Ravi Ramamoorthi. Vision transformer for nerf-based view synthesis from a single input image. In *WACV*, 2023.
- [29] Xinyue Liu, Xiangnan Kong, Lei Liu, and Kuorong Chiang. Treegan: syntax-aware sequence generation with generative adversarial networks. In *2018 IEEE International Conference on Data Mining (ICDM)*, pages 1140–1145. IEEE, 2018.
- [30] William E Lorensen and Harvey E Cline. Marching cubes: A high resolution 3d surface construction algorithm. *ACM siggraph computer graphics*, 21(4):163–169, 1987.
- [31] Quan Meng, Anpei Chen, Haimin Luo, Minye Wu, Hao Su, Lan Xu, Xuming He, and Jingyi Yu. Gnerf: Gan-based neural radiance field without posed camera. In *Proceedings of the IEEE/CVF International Conference on Computer Vision (ICCV)*, pages 6351–6361, October 2021.
- [32] Ben Mildenhall, Pratul P Srinivasan, Matthew Tancik, Jonathan T Barron, Ravi Ramamoorthi, and Ren Ng. Nerf: Representing scenes as neural radiance fields for view synthesis. *Communications of the ACM*, 65(1):99–106, 2021.
- [33] Norman Müller, Yawar Siddiqui, Lorenzo Porzi, Samuel Rota Bulò, Peter Kotschieder, and Matthias Nießner. Diffrf: Rendering-guided 3d radiance field diffusion. *arXiv preprint arXiv:2212.01206*, 2022.
- [34] Norman Müller, Andrea Simonelli, Lorenzo Porzi, Samuel Rota Bulò, Matthias Nießner, and Peter Kotschieder. Autorf: Learning 3d object radiance fields from single view observations. In *Proceedings of the IEEE/CVF Conference on Computer Vision and Pattern Recognition (CVPR)*, June 2022.
- [35] Thomas Müller, Alex Evans, Christoph Schied, and Alexander Keller. Instant neural graphics primitives with a multiresolution hash encoding. *ACM Trans. Graph.*, 41(4):102:1–102:15, July 2022.
- [36] Phuoc Nguyen, T. Tran, Ky Le, Sunil Gupta, Santu Rana, Dang Nguyen, Trong Nguyen, Shannon Ryan, and Svetha Venkatesh. Fast conditional network compression using bayesian hypernetworks. In *ECML/PKDD*, 2022.
- [37] Michael Niemeyer, Jonathan T Barron, Ben Mildenhall, Mehdi SM Sajjadi, Andreas Geiger, and Noha Radwan. Regnerf: Regularizing neural radiance fields for view synthesis from sparse inputs. In *Proceedings of the IEEE/CVF Conference on Computer Vision and Pattern Recognition*, pages 5480–5490, 2022.

- [38] Michael Oechsle, Songyou Peng, and Andreas Geiger. Unisurf: Unifying neural implicit surfaces and radiance fields for multi-view reconstruction. In *International Conference on Computer Vision (ICCV)*, 2021.
- [39] Jeong Joon Park, Peter Florence, Julian Straub, Richard Newcombe, and Steven Lovegrove. DeepSDF: Learning continuous signed distance functions for shape representation. In *Proceedings of the IEEE/CVF conference on computer vision and pattern recognition*, pages 165–174, 2019.
- [40] Ben Poole, Ajay Jain, Jonathan T. Barron, and Ben Mildenhall. DreamFusion: Text-to-3d using 2d diffusion. *arXiv*, 2022.
- [41] Alec Radford, Jong Wook Kim, Chris Hallacy, Aditya Ramesh, Gabriel Goh, Sandhini Agarwal, Girish Sastry, Amanda Askell, Pamela Mishkin, Jack Clark, et al. Learning transferable visual models from natural language supervision. In *International conference on machine learning*, pages 8748–8763. PMLR, 2021.
- [42] Ali Razavi, Aäron van den Oord, and Oriol Vinyals. Generating diverse high-fidelity images with vq-vae-2. *ArXiv*, abs/1906.00446, 2019.
- [43] Daniel Rebain, Mark Matthews, Kwang Moo Yi, Dmitry Lagun, and Andrea Tagliasacchi. Lohnerf: Learn from one look. In *Proceedings of the IEEE/CVF Conference on Computer Vision and Pattern Recognition*, pages 1558–1567, 2022.
- [44] Barbara Roessle, Jonathan T. Barron, Ben Mildenhall, Pratul P. Srinivasan, and Matthias Nießner. Dense depth priors for neural radiance fields from sparse input views. In *Proceedings of the IEEE/CVF Conference on Computer Vision and Pattern Recognition (CVPR)*, June 2022.
- [45] Mehdi SM Sajjadi, Henning Meyer, Etienne Pot, Urs Bergmann, Klaus Greff, Noha Radwan, Suhani Vora, Mario Lučić, Daniel Duckworth, Alexey Dosovitskiy, et al. Scene representation transformer: Geometry-free novel view synthesis through set-latent scene representations. In *Proceedings of the IEEE/CVF Conference on Computer Vision and Pattern Recognition*, pages 6229–6238, 2022.
- [46] Rahul Sajjani, Adrien Poulenard, Jivitesh Jain, Radhika Dua, Leonidas J. Guibas, and Srinath Sridhar. Condor: Self-supervised canonicalization of 3d pose for partial shapes. In *The IEEE Conference on Computer Vision and Pattern Recognition (CVPR)*, June 2022.
- [47] Katja Schwarz, Yiyi Liao, Michael Niemeyer, and Andreas Geiger. Graf: Generative radiance fields for 3d-aware image synthesis. In *Advances in Neural Information Processing Systems (NeurIPS)*, 2020.
- [48] Bipasha Sen, Aditya Agarwal, Vinay P Namboodiri, and C.V. Jawahar. INR-v: A continuous representation space for video-based generative tasks. *Transactions on Machine Learning Research*, 2022.
- [49] Bipasha Sen, Aditya Agarwal, Gaurav Singh, Brojeshwar B., Srinath Sridhar, and Madhava Krishna. Scarp: 3d shape completion in arbitrary poses for improved grasping. In *2023 IEEE International Conference on Robotics and Automation (ICRA)*, pages 3838–3845, 2023.
- [50] Marcin Sendera, Marcin Przewiezlikowski, Konrad Karanowski, Maciej Zieba, Jacek Tabor, and Przemysław Spurek. Hypershot: Few-shot learning by kernel hypernetworks. *2023 IEEE/CVF Winter Conference on Applications of Computer Vision (WACV)*, pages 2468–2477, 2022.
- [51] Anthony Simeonov, Yilun Du, Yen-Chen Lin, Alberto Rodriguez Garcia, Leslie Pack Kaelbling, Tomás Lozano-Pérez, and Pulkit Agrawal. SE(3)-equivariant relational rearrangement with neural descriptor fields. In *6th Annual Conference on Robot Learning*, 2022.
- [52] Anthony Simeonov, Yilun Du, Andrea Tagliasacchi, Joshua B. Tenenbaum, Alberto Rodriguez, Pulkit Agrawal, and Vincent Sitzmann. Neural descriptor fields: Se(3)-equivariant object representations for manipulation. 2022.
- [53] Samarth Sinha, Jason Y Zhang, Andrea Tagliasacchi, Igor Gilitschenski, and David B Lindell. Sparsepose: Sparse-view camera pose regression and refinement. *arXiv preprint arXiv:2211.16991*, 2022.
- [54] Vincent Sitzmann, Julien Martel, Alexander Bergman, David Lindell, and Gordon Wetzstein. Implicit neural representations with periodic activation functions. *Advances in Neural Information Processing Systems*, 33:7462–7473, 2020.

- [55] Vincent Sitzmann, Semon Rezchikov, Bill Freeman, Josh Tenenbaum, and Fredo Durand. Light field networks: Neural scene representations with single-evaluation rendering. *Advances in Neural Information Processing Systems*, 34:19313–19325, 2021.
- [56] Vincent Sitzmann, Michael Zollhoefer, and Gordon Wetzstein. Scene representation networks: Continuous 3d-structure-aware neural scene representations. In H. Wallach, H. Larochelle, A. Beygelzimer, F. d'Alché-Buc, E. Fox, and R. Garnett, editors, *Advances in Neural Information Processing Systems*, volume 32. Curran Associates, Inc., 2019.
- [57] Ivan Skorokhodov, Savva Ignatyev, and Mohamed Elhoseiny. Adversarial generation of continuous images. In *Proceedings of the IEEE/CVF Conference on Computer Vision and Pattern Recognition*, pages 10753–10764, 2021.
- [58] Ivan Skorokhodov, Sergey Tulyakov, and Mohamed Elhoseiny. Stylegan-v: A continuous video generator with the price, image quality and perks of stylegan2. In *Proceedings of the IEEE/CVF Conference on Computer Vision and Pattern Recognition*, pages 3626–3636, 2022.
- [59] Cheng Sun, Min Sun, and Hwann-Tzong Chen. Direct voxel grid optimization: Super-fast convergence for radiance fields reconstruction. In *Proceedings of the IEEE/CVF Conference on Computer Vision and Pattern Recognition*, pages 5459–5469, 2022.
- [60] Matthew Tancik, Vincent Casser, Xinchun Yan, Sabeek Pradhan, Ben Mildenhall, Pratul P Srinivasan, Jonathan T Barron, and Henrik Kretzschmar. Block-nerf: Scalable large scene neural view synthesis. In *Proceedings of the IEEE/CVF Conference on Computer Vision and Pattern Recognition*, pages 8248–8258, 2022.
- [61] Matthew Tancik, Ben Mildenhall, Terrance Wang, Divi Schmidt, Pratul P. Srinivasan, Jonathan T. Barron, and Ren Ng. Learned initializations for optimizing coordinate-based neural representations. In *CVPR*, 2021.
- [62] Ayush Tewari, Justus Thies, Ben Mildenhall, Pratul Srinivasan, Edgar Tretschk, Wang Yifan, Christoph Lassner, Vincent Sitzmann, Ricardo Martin-Brualla, Stephen Lombardi, et al. Advances in neural rendering. In *Computer Graphics Forum*, volume 41, pages 703–735. Wiley Online Library, 2022.
- [63] Johannes Von Oswald, Christian Henning, João Sacramento, and Benjamin F Grewe. Continual learning with hypernetworks. *arXiv preprint arXiv:1906.00695*, 2019.
- [64] Can Wang, Menglei Chai, Mingming He, Dongdong Chen, and Jing Liao. Clip-nerf: Text-and-image driven manipulation of neural radiance fields. In *Proceedings of the IEEE/CVF Conference on Computer Vision and Pattern Recognition*, pages 3835–3844, 2022.
- [65] He Wang, Srinath Sridhar, Jingwei Huang, Julien Valentin, Shuran Song, and Leonidas J. Guibas. Normalized object coordinate space for category-level 6d object pose and size estimation. In *The IEEE Conference on Computer Vision and Pattern Recognition (CVPR)*, June 2019.
- [66] Peng Wang, Lingjie Liu, Yuan Liu, Christian Theobalt, Taku Komura, and Wenping Wang. Neus: Learning neural implicit surfaces by volume rendering for multi-view reconstruction. *NeurIPS*, 2021.
- [67] Zirui Wang, Shangzhe Wu, Weidi Xie, Min Chen, and Victor Adrian Prisacariu. NeRF—: Neural radiance fields without known camera parameters. *arXiv preprint arXiv:2102.07064*, 2021.
- [68] Francis Williams, Zan Gojcic, Sameh Khamis, Denis Zorin, Joan Bruna, Sanja Fidler, and Or Litany. Neural fields as learnable kernels for 3d reconstruction. In *Proceedings of the IEEE/CVF Conference on Computer Vision and Pattern Recognition*, pages 18500–18510, 2022.
- [69] Yuanbo Xiangli, Linning Xu, Xingang Pan, Nanxuan Zhao, Anyi Rao, Christian Theobalt, Bo Dai, and Dahua Lin. Citynerf: Building nerf at city scale. *arXiv preprint arXiv:2112.05504*, 2021.
- [70] Yiheng Xie, Towaki Takikawa, Shunsuke Saito, Or Litany, Shiqin Yan, Numair Khan, Federico Tombari, James Tompkin, Vincent Sitzmann, and Srinath Sridhar. Neural fields in visual computing and beyond. *Computer Graphics Forum*, 2022.
- [71] DeJia Xu, Yifan Jiang, Peihao Wang, Zhiwen Fan, Humphrey Shi, and Zhangyang Wang. Sinnerf: Training neural radiance fields on complex scenes from a single image. In *Computer Vision—ECCV 2022: 17th European Conference, Tel Aviv, Israel, October 23–27, 2022, Proceedings, Part XXII*, pages 736–753. Springer, 2022.

- [72] Lior Yariv, Jiatao Gu, Yoni Kasten, and Yaron Lipman. Volume rendering of neural implicit surfaces. In *Thirty-Fifth Conference on Neural Information Processing Systems*, 2021.
- [73] Alex Yu, Sara Fridovich-Keil, Matthew Tancik, Qinhong Chen, Benjamin Recht, and Angjoo Kanazawa. Plenoxels: Radiance fields without neural networks. *arXiv preprint arXiv:2112.05131*, 2021.
- [74] Alex Yu, Ruilong Li, Matthew Tancik, Hao Li, Ren Ng, and Angjoo Kanazawa. Plenotrees for real-time rendering of neural radiance fields. In *Proceedings of the IEEE/CVF International Conference on Computer Vision*, pages 5752–5761, 2021.
- [75] Alex Yu, Vickie Ye, Matthew Tancik, and Angjoo Kanazawa. pixelNeRF: Neural radiance fields from one or few images. In *CVPR*, 2021.
- [76] Sihyun Yu, Jihoon Tack, Sangwoo Mo, Hyunsu Kim, Junho Kim, Jung-Woo Ha, and Jinwoo Shin. Generating videos with dynamics-aware implicit generative adversarial networks. *ArXiv*, abs/2202.10571, 2022.
- [77] Biao Zhang, Jiapeng Tang, Matthias Niessner, and Peter Wonka. 3dshape2vecset: A 3d shape representation for neural fields and generative diffusion models. *arXiv preprint arXiv:2301.11445*, 2023.
- [78] Richard Zhang, Phillip Isola, Alexei A Efros, Eli Shechtman, and Oliver Wang. The unreasonable effectiveness of deep features as a perceptual metric. In *CVPR*, 2018.
- [79] Peng Zhou, Lingxi Xie, Bingbing Ni, and Qi Tian. CIPS-3D: A 3D-Aware Generator of GANs Based on Conditionally-Independent Pixel Synthesis. 2021.

A Experiments

		Chairs			Sofa		
		PSNR \uparrow	SSIM \uparrow	LPIPS \downarrow	PSNR \uparrow	SSIM \uparrow	LPIPS \downarrow
ABO	PixelNeRF [75]	19.00	0.74	0.343	18.49	0.77	0.351
	CodeNeRF [19]	20.51	0.75	0.264	20.38	0.77	0.31
	HyP-NeRF (Ours)	25.92	0.91	0.093	26.73	0.91	0.098
	w/o denoising	24.83	0.87	0.12	25.68	0.87	0.14

Table 5: **Generalization.** Comparison of single-view NeRF generation on the ABO dataset. Metrics are computed on renderings of resolution 128×128 . HyP-NeRF significantly outperforms PixelNeRF [75] and CodeNeRF [19] on all of the metrics in both object categories.

A.1 Additional Architectural Details

We provide the network architecture in the main paper, Section 4. During training, we use Adam Optimizer, with a learning rate of $1e - 3$ with $\beta_1 = 0.9$ and $\beta_2 = 0.99$, along with a lambda LR scheduler³. We use the PyTorch implementation InstantNGP⁴ and provide the training, inference, and metric computation code in the Appendix.

A.2 Metrics and Additional Comparisons

To the best of our knowledge, we are the first work to perform single-view NeRF generation at a resolution of 512×512 . Therefore, we set a benchmark on the ABO dataset against PixelNeRF in the main paper, Table 1. However, it is worth noting that PixelNeRF was originally trained at a resolution of 128×128 . Therefore, we also compare with PixelNeRF on ABO at a resolution of 128×128 in the Appendix, Table 5 and Figure 9. To do so, we retrain PixelNeRF on 128×128 by downsampling the ground truth datapoints in ABO. Further, we show qualitative results in the main paper on SRN [56] against VisionNeRF [28], FE-NVS [14], CodeNeRF [19], and PixelNeRF at 128×128 . In the Appendix, we show quantitative results in Table 6. Lastly, in Table 7, we show additional ablation on Denoise and Finetune (see main paper, Section 3.1-Step 2). In this table, we primarily evaluate the geometric consistency before and after the denoising step. As explained in the main paper, Section 4, we use Chamfer’s Distance (CD \downarrow) to compute the geometric consistency.

To compute CD, we first train the ground truth NeRFs by optimizing InstantNGP [35] on the multiview ground truths. Next, we render meshes from InstantNGP’s and HyP-NeRF’s predicted NeRF using torch-ngp’s save_mesh() implementation⁵. From the rendered mesh, we sample 4096 points uniformly and compute CD between both the pointclouds. **We encourage the readers to view the supplementary video for the best experience of the qualitative results.**

A.3 Generalization

To ensure that HyP-NeRF can model novel NeRF instances unseen at the time of training, we rely on the conditional task of “single-view NeRF generation”. In the main paper, we show experiments on ABO dataset at 512×512 resolution; in the Appendix, we make comparisons on a lower resolution of 128×128 on ABO against PixelNeRF in Table 5 and on SRN against the existing baselines in Table 6. As can be seen, we significantly outperform PixelNeRF on the ABO dataset and perform comparably with the existing baselines on the SRN dataset. **Note** that we do not employ the Denoise and Finetune step (see main paper, Section 3.1) in SRN. However, another reason for our low performance on SRN (when compared to ABO) is the difference in the views adopted in ABO and SRN. ABO renders the 3D structure from 91 viewpoints on the upper icosphere with varying azimuth and elevation [11]. SRN, on the other hand, renders the upper along with the lower icosphere. This includes viewpoints from the absolute bottom and top parts of the object providing insufficient context for test-time optimization.

We observe that, in practice, our output quality improves significantly as we increase the number of viewpoints on SRN as shown qualitatively in Figure 10. This indicates that although HyP-NeRF has

³https://pytorch.org/docs/stable/generated/torch.optim.lr_scheduler.LambdaLR.html

⁴<https://github.com/ashawkey/torch-ngp>

⁵<https://github.com/ashawkey/torch-ngp/blob/main/nerf/utils.py>

		Chairs			Cars		
		PSNR \uparrow	SSIM \uparrow	LPIPS \downarrow	PSNR \uparrow	SSIM \uparrow	LPIPS \downarrow
SRN	PixelNeRF [75]	23.72	0.90	0.128	23.17	0.89	0.146
	CodeNeRF [19]	23.39	0.87	0.166	22.73	0.89	0.128
	FE-NVS [14]	23.21	0.92	0.077	22.83	0.91	0.099
	VisionNeRF [28]	24.48	0.92	0.077	22.88	0.90	0.084
	HyP-NeRF	22.80	0.88	0.13	23.48	0.91	0.09
w/o Denoise		21.02	0.87	0.14	21.30	0.88	0.111

Table 6: **Generalization.** Comparison of single-view NeRF generation on the SRN dataset. Metrics are computed on renderings of resolution 128×128 . Results of all the models (except HyP-NeRF) are taken from the official papers. HyP-NeRF performs comparably with the existing baselines. Note, we do not incorporate the second step of HyP-NeRF, Denoise and Finetune (main paper, Section 3.1).

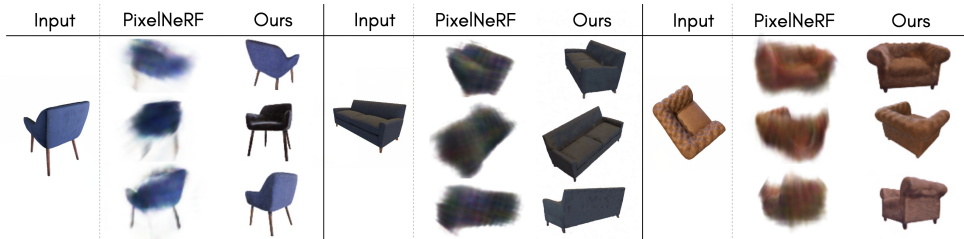


Figure 9: **Qualitative results of single-view NeRF generation** on ABO dataset at a resolution of 128×128 . HyP-NeRF preserves fine details even at this low resolution. PixelNeRF improves in quality when compared to 512×512 (see main paper, Figure 4). However, it still struggles to model the fine texture and shape details in the ABO dataset and performs subpar to HyP-NeRF.



Figure 10: **Multiview test-time optimization on SRN Chairs.** HyP-NeRF can perform test-time optimization (see main paper, Section 3.1) with any number of views. In this qualitative result, we start with an instance that did not optimize well through a single pose (because of a challenging viewpoint) and show the improvement in quality of the generated NeRF as we increase the number of views (ie. coverage) for optimization. The header indicate the number of views used for the optimization. As shown, the difference in quality between five and ten poses is insignificant. The rightmost result shows drastic improvement in the render quality from one to three views showcasing the impact of pose on test-time optimization.

modeled this particular NeRF instance, it is hard to find the NeRF through single-view optimization suggesting the need for a more robust mechanism to map to HyP-NeRF’s prior.

It is also worth noting that, PixelNeRF and VisionNeRF (trained on 16 NVIDIA A100 for 5 days) are designed specifically for the task single-view NeRF generation. Whereas, we aim to train a prior and use this conditional task to validate that our learned prior can model novel instances unseen at the time of training. Further, as can be seen in Table 5, HyP-NeRF significantly outperforms PixelNeRF on the challenging ABO dataset with high-fidelity structure and texture, indicating that HyP-NeRF is capable of modeling datasets made of fine textures and shapes as found in the real-world, that the existing work (PixelNeRF) struggle to train on.

B Additional Ablations

Impact of Resolution on the Quality: As we operate directly in the NeRF space, we can essentially render the NeRFs in any resolution. In this ablation, we measure the quality of our renderings at different resolutions as shown in Figure 11. To generate the ground truth, we perform interarea downsampling on the ABO datapoints. As expected, HyP-NeRF generates high-quality NeRF in

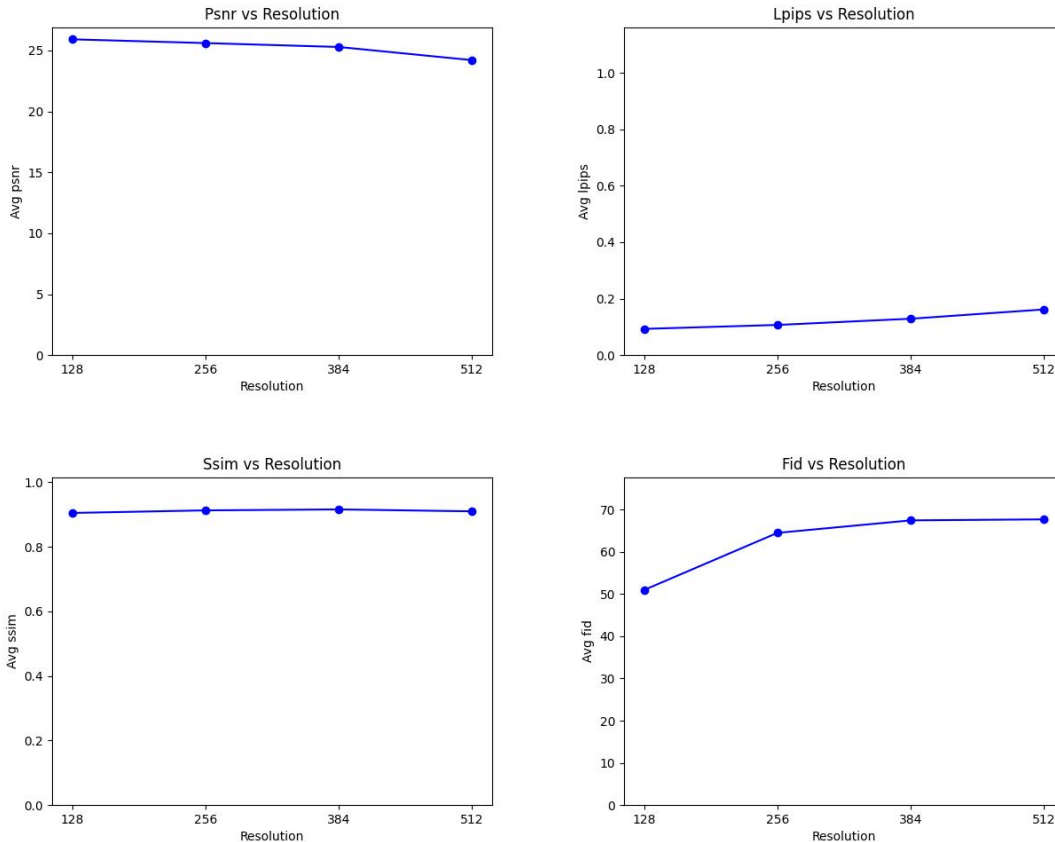


Figure 11: **Performance of HyP-NeRF on multiple resolutions.** As HyP-NeRF operates directly in the NeRF space, it can render the NeRFs in potentially any resolution. In this plot, we showcase HyP-NeRF’s performance rendered in different resolutions. As can be seen, the quality does not degrade with the resolution and HyP-NeRF performs well consistently.

each resolution, and the quality does not degrade with the rendered resolution. As ABO consists of rendering at a resolution of 512×512 , we only make comparisons on the lower resolutions as bicubic upsampling on the ground truth would reduce the quality of the ground truth itself. However, to showcase our quality on higher resolution, we present our rendering at 1024×1024 in the supplementary video, timestamp 01:17.

Geometric Consistency on Denoising: As explained in the main paper, Section 3.1, we perform Denoise and Finetune by first projecting the NeRF into predefined multiview images, followed by performing image-level denoising frame-by-frame. As we only finetune an already multiview and geometrically consistent NeRF, we observed that the finetuning is robust to minor denoised image-level multiview inconsistencies. We showcase this qualitatively in the supplementary video (timestamps 3:05-3:30), in the main paper-Figure 4, and in the Appendix-Figure 13 and Figure 14. In this section, we quantitatively evaluate the geometric consistency using the CD metric as defined in Appendix A.2. The results are presented in Table 7, and as expected, there is no degradation in the quality between HyP-NeRF’s output before and after the Denoise and Finetune process, clearly showcasing that the geometric consistency is not affected even though we only rely on a simple frame-by-frame denoising.

	Chairs CD ↓
HyP-NeRF	
with D&F	0.0062
without D&F	0.0064

Table 7: **Denoise and Finetune (D&F) ablation (see main paper (Section 3.1 Step 2)).** We evaluate the geometric consistency using CD↓ metric defined in Appendix A.2.

C Qualitative Results

In this section, we show the qualitative results in higher resolution. Figure 12 presents the comparison between InstantNGP, trained on a single instance, against HyP-NeRF trained on thousands of NeRF

instances, thereby compressing the instances to a single network (see the main paper, Section 4.2). Figure 13 and Figure 14 present qualitative results on inversion and highlight the difference before and after the Denoise and Finetune step (see main paper, Section 3.1).



Figure 12: **Qualitative comparison on Compression.** We compare against InstantNGP [35], which is trained for a specific instance. On the other hand, HyP-NeRF is trained on thousands of NeRF instances. Despite that, HyP-NeRF has learned to generate the NeRFs and essentially compress them almost losslessly. See the main paper, Section 4.2, for more details.



Figure 13: **Qualitative Results on Generalization.** We perform test-test optimization (see the main paper, Section 3.2) to generate NeRFs from a single input view. Our Denoise and Finetune step (see the main paper, Section 3.1) significantly improves the texture and the edges by making it smooth and even.



Figure 14: **Qualitative Results on Generalization.** We perform test-test optimization (see the main paper, Section 3.2) to generate NeRFs from a single input view. Denoise and Finetune (see the main paper, Section 3.1) improves the quality of the outputs, for example, the legs are clearly more evened out and noiseless in the bottom example. The difference is, however, less drastic in the top example.